Strong spin-orbit interactions and weak antilocalization in carbon-doped *p*-type GaAs/$Al_xGa_{1-x}As$ heterostructures

Boris Grbić,[1] Renaud Leturcq,[1] Thomas Ihn,[1] Klaus Ensslin,[1] Dirk Reuter,[2] and Andreas D. Wieck[2]
[1]*Solid State Physics Laboratory, ETH Zurich, 8093 Zurich, Switzerland*
[2]*Angewandte Festkörperphysik, Ruhr-Universität Bochum, 44780 Bochum, Germany*

(Received 30 October 2007; revised manuscript received 10 February 2008; published 10 March 2008)

We present a comprehensive study of the low-field magnetoresistance in carbon-doped *p*-type GaAs/AlGaAs heterostructures aiming at the investigation of spin-orbit interaction effects. The following signatures of exceptionally strong spin-orbit interactions are simultaneously observed: a beating in the Shubnikov–de Haas oscillations, a classical positive magnetoresistance due to the presence of the two spin-split subbands, and a weak antilocalization dip in the magnetoresistance. The spin-orbit-induced splitting of the heavy hole subband at the Fermi level is determined to be around 30% of the total Fermi energy. The phase-coherence length of holes of around 2.5 μm at a temperature of 70 mK, extracted from weak antilocalization measurements, is promising for the fabrication of phase-coherent *p*-type nanodevices.

DOI: 10.1103/PhysRevB.77.125312 PACS number(s): 73.20.Fz, 71.70.Ej, 73.61.Ey, 72.20.Fr

I. INTRODUCTION

Two-dimensional systems with strong spin-orbit interactions (SOIs) are promising for the realization of spintronic devices due to the fact that in such systems, the electron (hole) spin could be affected, not only by magnetic but also by electric fields.[1,2] SOIs are expected to be very strong in *p*-type GaAs heterostructures, due to the high effective mass of holes,[3] which makes the ratio of the SOI energy and the kinetic energy larger in the valence than in the conduction band. As a result of the SOI, the heavy hole subband in GaAs is split into two subbands even in the absence of an external magnetic field.

In magnetotransport experiments, the existence of two spin-split subbands with different mobilities results in a classical positive magnetoresistance. In addition, a beating can be observed in Shubnikov–de Haas (SdH) oscillations because the Landau levels of the two nonequally populated subbands give rise to magnetoresistance oscillations with slightly different $1/B$ periodicities.[4] While these two signatures can be observed in any two-subband system, the spin splitting due to SOI can be unambiguously identified and characterized by measurements of the weak antilocalization effect.

Weak localization is a quantum mechanical effect, which arises from the constructive interference between time-reversed partial waves of the charge carriers in disordered materials. It leads to an enhanced probability of carrier backscattering and, therefore, to an enhanced longitudinal resistivity. This interference effect is relevant for diffusive orbits up to the length scale l_ϕ, the phase-coherence length. The application of a magnetic field normal to the plane of carrier motion breaks the time reversal symmetry, suppresses the weak localization, and, therefore, leads to a negative magnetoresistance at low magnetic fields around $B=0$.[5]

In systems with strong SOI, the spin dynamics of the carriers is coupled to their orbital motion and the interference of time-reversed paths has consequences beyond the weak localization effect. As the spin experiences a sequence of scattering events along its path, the spin orientation is randomized on a characteristic length scale l_{so}. The stronger the SOI, the smaller is l_{so}. At $B=0$, the interference of time-reversed paths leads to a reduction of the backscattering probability below its classical value,[6] an effect called weak antilocalization, if $l_{so} \ll l_\phi$ (strong SOI). It manifests itself as a positive (rather than a negative) magnetoresistance at small fields around $B=0$.[7]

Weak antilocalization was experimentally observed by Bergmann in thin metallic films.[8] As the strength of SOI is increased, a transition from weak localization to weak antilocalization is observed. Weak antilocalization was subsequently observed also in semiconductor heterostructures.[9,10] A smaller zero-field antilocalization resistance minimum superimposed on a larger weak localization peak was seen in the magnetoresistance of an inversion layer of InP,[9] and an *n*-type GaAs/AlGaAs heterostructure.[10] A fully developed antilocalization minimum was observed by Chen *et al.* in the magnetoresistance of an InAs quantum well.[11] Koga *et al.* demonstrated the transition from a zero-field weak localization maximum to a weak antilocalization minimum by tuning the symmetry of an InGaAs quantum well with a metallic top gate.[12]

Weak antilocalization is expected to be particularly expressed in the case of *p*-type GaAs heterostructures due to the strong SOI in these systems. Experimental studies of weak antilocalization in Be-doped (100) *p*-type GaAs heterostructures are reported in Refs. 13 and 14, and a detailed study of the low-field magnetoresistance in Si-doped (311) *p*-type GaAs heterostructures is presented in Ref. 15.

Here, we report measurements of the classical positive magnetoresistance, SdH oscillations, and weak antilocalization in C-doped *p*-type GaAs heterostructures. Weak antilocalization is typically more pronounced in diffusive, low-mobility samples, while for the observation of beating in SdH oscillations, higher mobility samples are required. The fact that our sample is in the regime of intermediate mobilities enables us to simultaneously observe both effects and to perform a complementary analysis of spin-orbit interactions in the system. The observation of a fully developed antilocalization minimum around $B=0$ clearly demonstrates the

 ©2008 The American Physical Society

presence of very strong SOI. A phase-coherence time of the holes of around 190 ps, corresponding to a phase-coherence length of 2.5 μm is extracted from these measurements. We investigate the temperature dependence of the phase-coherence time of holes and find that it obeys a $1/T$ dependence with reasonable accuracy. Limitations in extracting the spin-orbit scattering time are due to the fact that SOI is very strong. It cannot be treated as a weak perturbation only, as discussed below.

II. SAMPLE AND MEASUREMENT SETUP

We have studied the low-field magnetoresistance in two C-doped *p*-type GaAs/AlGaAs heterostructures with the two-dimensional hole gas (2DHG) buried 45 and 100 nm below the surface. The results obtained from both samples are qualitatively the same. For the sake of clarity, we present here results obtained on the sample with the 2DHG formed at the interface 100 nm below the sample surface. The heterostructure consists of a 5 nm C-doped GaAs cap layer, followed by a 65 nm thick, homogeneously C-doped layer of $Al_{0.31}Ga_{0.69}As$, which is separated from the 2DHG by a 30 nm thick, undoped $Al_{0.31}Ga_{0.69}As$ spacer layer.[16] A rectangular Hall bar was fabricated by standard photolithography. Its width is 100 μm and the separation between adjacent voltage leads is 500 μm. Ohmic contacts were formed by evaporating Au and Zn and subsequent annealing at 480 °C for 2 min. Afterward, a homogeneous Ti/Au top gate was evaporated, which allows us to tune the density in the range of $(2-3)\times 10^{11}$ cm^{-2}. The average mobility in the sample at T=70 mK is 160 000 cm^2/V s at a density of 3×10^{11}cm^{-2}. The high quality of the investigated sample has been demonstrated by the observation of the fractional and integer quantum Hall effects, as well as by measurements of highly resolved SdH oscillations.[17]

The Hall bar is fabricated along one of the two main crystallographic directions in the (100) plane. Measurements at T=4.2 K on another sample fabricated from the same wafer patterned into an L-shaped Hall bar have shown that the mobility anisotropy between the two main crystallographic directions in the (100) plane is less than 25%,[18] which is significantly less than in Si-doped (311) *p*-type GaAs heterostructures.[19] Therefore, in contrast to *p*-type GaAs samples on (311) substrates, where the mobility anisotropy had to be invoked for the interpretation of the low-field magnetoresistance,[15] in our measurements on (100) *p*-type GaAs samples, the mobility anisotropy could be neglected.

We have performed four-terminal measurements of the resistivity using standard low-frequency lock-in techniques. A current of 20 nA was driven through the Hall bar at a frequency of 31 Hz, and the voltage was measured with an integration time of 300 ms. In order to improve the signal-to-noise ratio, we used a voltage amplifier with an amplification of 1000 directly at the outputs of the cryostat. In order to increase the signal-to-noise ratio further in measurements of the weak antilocalization effect, each data point is the average of 25 samples taken with a temporal separation of 1.5 s. In this way, we reached a noise level of less than 0.03 Ω for measured resistances above 200 Ω. For these

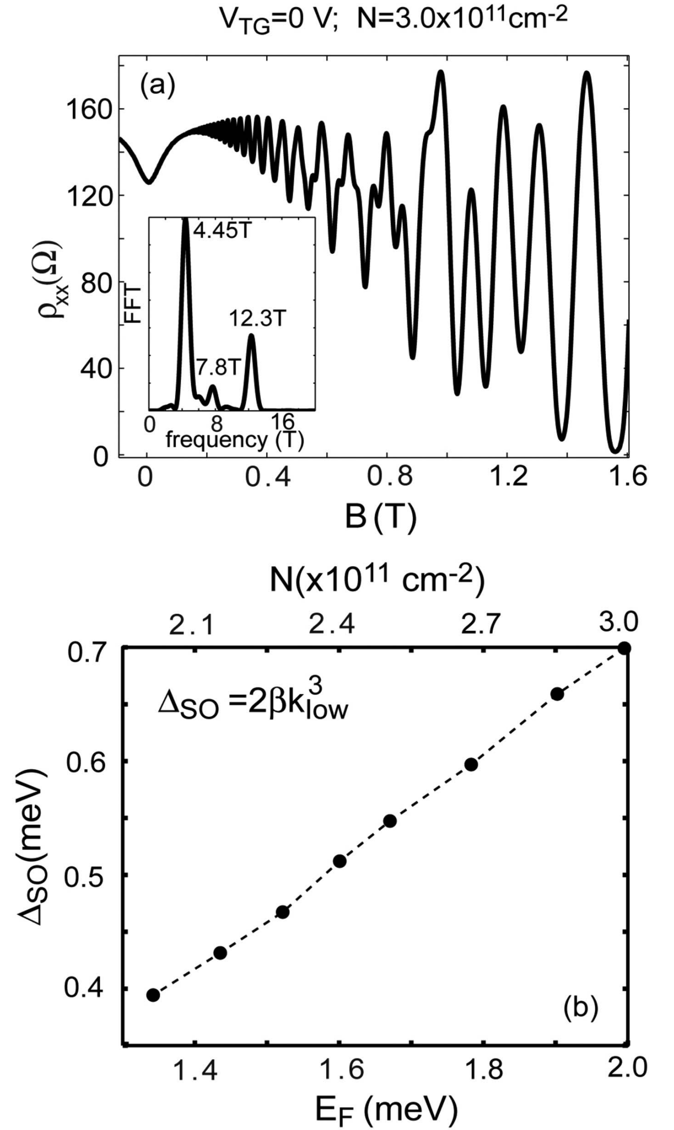

FIG. 1. (a) Shubnikov–de Haas oscillations in the magnetoresistance, with a top gate set to V_{TG}=0 V and the total density 3.0×10^{11} cm^{-2}. Inset: Fourier transform of the shown magnetoresistance, taken in the B-field range (0.4, 1.5 T) displaying three peaks. (b) Spin-orbit splitting energy of the heavy hole subband at the Fermi level as a function of the Fermi energy in the system and the total density.

measurements, a special homebuilt power supply for the magnet was used, and the magnetic field is stepped with a resolution of 40 μT.

III. BEATING OF SHUBNIKOV–DE HAAS OSCILLATIONS

We have mentioned before that the two spin-split heavy hole subbands arising as a result of SOI lead to a beating of SdH oscillations. Figure 1(a) displays a magnetoresistance trace taken in the magnetic field range between −0.1 and 1.6 T showing SdH oscillations. The Fourier analysis of the magnetoresistivity ρ_{xx} vs $1/B$ [see inset of Fig. 1(a) and discussion below] is used to deduce the densities $N_{1,2}$ of the two

spin-split subbands. They are related to the two frequencies $f_{1,2}$ obtained from the Fourier transform of the SdH oscillations via $N_{1,2}=(e/h)f_{1,2}$,[3,4,20] within the semiclassical approximation. An analysis beyond this approximation requires a numerical $\mathbf{k}\cdot\mathbf{p}$ approach, which is beyond the scope of our analysis.

Three magnetic field regimes can be identified in the raw data, where SdH oscillations exhibit a different behavior. For very low fields in the interval $0.2\ \mathrm{T}<B<0.4\ \mathrm{T}$, only SdH oscillations originating from the higher mobility spin-split subband are observed, allowing to extract its density. As the magnetic field is further increased into the region between $0.4\ \mathrm{T}<B<2\ \mathrm{T}$, the contribution from the second spin-split subband becomes visible in the oscillations. The Fourier transform analysis of the data in this range result in a spectrum with three peaks corresponding to the populations of each of the two spin-split subbands and to the total density. An example of such a Fourier transform spectrum obtained from data in the range $0.4\ \mathrm{T}<B<1.5\ \mathrm{T}$ is shown in the inset of Fig. 1(a). Three peaks (at 4.45, 7.8, and 12.3 T) can be seen. The relation $f_1+f_2=f_{tot}$, which reflects the fact that the two-subband densities sum up to the total density, is reasonably satisfied. For magnetic fields above approximately 2 T (not shown), we observe magnetoresistance oscillations related to the total density in the system, and only the total density peak is present in the Fourier spectrum.

From the three peaks in the Fourier transform shown in the inset of Fig. 1(a), we read the densities of the two spin-split subbands, $N_1=1\times10^{11}\ \mathrm{cm}^{-2}$ and $N_2=1.9\times10^{11}\ \mathrm{cm}^{-2}$, and the total density, $N=3\times10^{11}\ \mathrm{cm}^{-2}$. This corresponds to a relative charge imbalance between the two spin-split subbands $\Delta N/N=0.30$. The strength of the spin-orbit interactions can be quantified using this relative charge imbalance, if a cubic wave vector k dependence $\Delta_{\mathrm{SO}}=2\beta k_{\|}^3$ is assumed for heavy holes in the (100) plane.[3,21] The two subband's Fermi wave vectors k_1 and k_2 are different. This difference increases with increasing spin-orbit interaction. From the general relation $k_i=\sqrt{4\pi N_i}$, we find $k_1=1.1\times10^8\ \mathrm{m}^{-1}$ and $k_2=1.6\times10^8\ \mathrm{m}^{-1}$ at the total density $N=3\times10^{11}\ \mathrm{cm}^{-2}$. The energy splitting of the two spin-split subbands depends on the k vector where this splitting is calculated. The values of the spin-splitting energy which we quote further in the text are all obtained using the smaller of the two wave vectors and, therefore, represent the lower bound for the spin splitting of the heavy hole subband.

Using the masses of the carriers in the two spin-split subbands determined experimentally in Ref. 17 and the two-subband densities, we calculate the spin-orbit coupling parameter from Eq. (6.39) in Ref. 3 to be $\beta=2.5\times10^{-28}\ \mathrm{eV\ m}^3$. This gives the spin-orbit-induced splitting of the heavy hole subband $\Delta_{\mathrm{SO}}\approx0.7$ meV at a density $N=3\times10^{11}\ \mathrm{cm}^{-2}$. The Fermi energy for this density is $E_F=2.0$ meV. As a consequence, the strength of the spin-orbit interaction relative to the kinetic energy is $\Delta_{\mathrm{SO}}/E_F\approx35\%$. In the gate voltages shown in Fig. 1(b), the parameter β increases with increasing density by about 20%.

The evolution of the spin-splitting energy Δ_{SO} upon changing the total density in the system with the metallic top gate is shown in Fig. 1(b). It can be seen that for densities in the range of $(2-3)\times10^{11}\ \mathrm{cm}^{-2}$, the spin-splitting energy is in the range of 0.4–0.7 meV. Thus, the relative strength of spin-orbit interactions compared to the Fermi energy, Δ_{SO}/E_F, is quite large, increasing from 0.29 to 0.35 with the Fermi energy increasing from 1.35 to 2 meV. This documents the presence of exceptionally strong SOI in the C-doped p-GaAs heterostructure studied in this paper, which originates from the (100) orientation of the interface and the asymmetry of the confinement potential. Large SOI has also been observed before in (100)-oriented Be-doped samples.[22,23]

IV. CLASSICAL POSITIVE MAGNETORESISTANCE

The longitudinal magnetoresistance of a system with two types of charge carriers with different mobilities is parabolic around zero magnetic field, whereas the Hall resistivity contains a small cubic correction at low fields in addition to the usual term linear in B. This is a purely classical effect and follows from the standard Drude theory of conductivity.[24] If intersubband scattering between the two subbands is significant, a more complex theory based on the Boltzmann transport equation has to be considered.[25] However, the qualitative behavior of the low-field magnetoresistance remains very similar to that obtained using the simpler model neglecting intersubband scattering.

In the transport theory of two-subband systems developed by Zaremba,[25] where intersubband scattering is included, the longitudinal and transverse magnetoresistivities are given by

$$\rho_{xx}=\frac{m^*}{e^2}\,\mathrm{Re}\left[\frac{1}{\mathrm{Tr}\,\mathbf{N}(\mathbf{K}-i\omega_c\mathbf{I})^{-1}}\right], \tag{1}$$

$$\rho_{xy}=\frac{m^*}{e^2}\,\mathrm{Im}\left[\frac{1}{\mathrm{Tr}\,\mathbf{N}(\mathbf{K}-i\omega_c\mathbf{I})^{-1}}\right], \tag{2}$$

where Tr stands for the trace operation, $\mathbf{I}$ is the 2×2 unit matrix, $\mathbf{N}$ is a matrix defined as $N_{ij}=\sqrt{N_iN_j}$ (N_1, N_2 are the densities of the two subbands), and $\mathbf{K}$ is the scattering matrix

$$\begin{pmatrix} K_1 & -K_{12} \\ -K_{12} & K_2 \end{pmatrix},$$

where K_1, K_2 are rates quantifying intrasubband scattering, while K_{12} is the intersubband scattering rate.

Previously, a strong positive magnetoresistance was observed in p-type (311) GaAs heterostructures.[15] However, in that case, the low-field magnetoresistance could not be fitted satisfactorily with the two-subband theory, even when intersubband scattering was taken into account. This finding was attributed to the strong mobility anisotropy in (311) samples.

Figure 2 shows a strong positive magnetoresistance around $B=0$ in two gate configurations: (a1) $V_{\mathrm{TG}}=0$, $N=3.0\times10^{11}\ \mathrm{cm}^{-2}$ and (b1) $V_{\mathrm{TG}}=1$ V, $N=2.3\times10^{11}\ \mathrm{cm}^{-2}$. The black lines correspond to the measured data, while the thicker gray lines show the fits following Eq. (1) in the range $|B|<0.15$ T for $V_{\mathrm{TG}}=0$ and $|B|<0.2$ T for $V_{\mathrm{TG}}=1$ V, where SdH oscillations are not yet developed. In the fitting procedure, the densities of the two subbands N_1, N_2 are fixed parameters given from the Fourier analysis of the SdH oscilla-

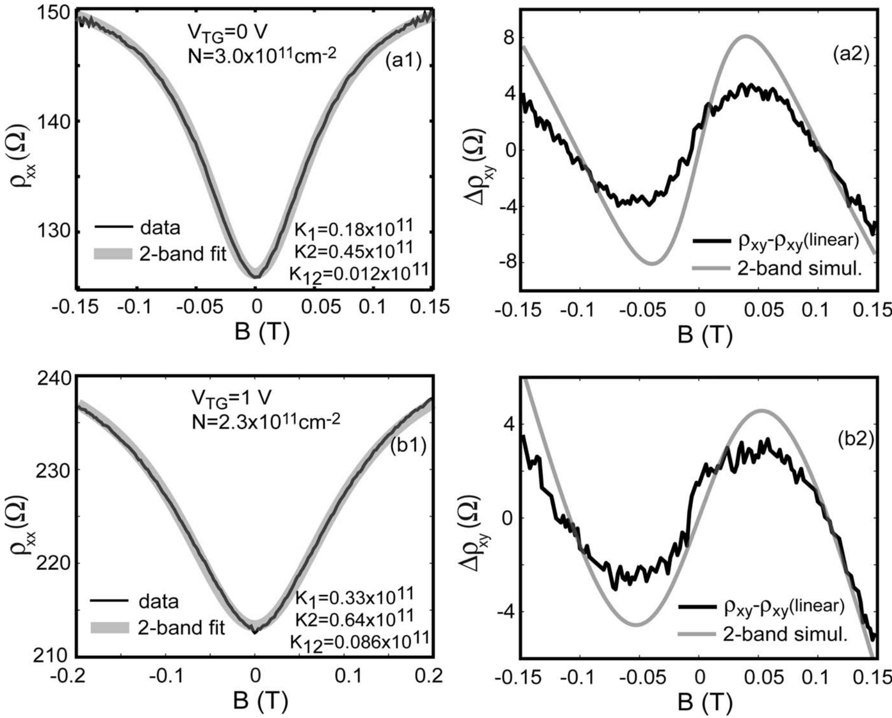

FIG. 2. Left column: Fit of the low-field magnetoresistivity with the two-band theory (Ref. 25) (black lines represent the measurement and thicker gray lines are fitted lines) in the following gate configurations: (a1) $V_{TG}=0$, $N=3.0\times10^{11}$ cm^{-2}; (b1) $V_{TG}=1$ V, $N=2.3\times10^{11}$ cm^{-2}. Values for K_1, K_2, and K_{12} are given in units 1/s. Right column: Nonlinearity in the low-field Hall resistivity (black lines are measured data and gray lines are calculated curves; see text for detailed explanations) in the following gate configurations: (a2) $V_{TG}=0$, $N=3.0\times10^{11}$ cm^{-2}; (b2) $V_{TG}=1$ V, $N=2.3\times10^{11}$ cm^{-2}.

tions, whereas the scattering rates K_1, K_2, K_{12} are fitting parameters.

In the configuration $V_{TG}=0$, $N=3.0\times10^{11}$ cm^{-2} [Fig. 2(a1)], the scattering rates are $K_1=0.018$ ps^{-1}, $K_2=0.045$ ps^{-1}, and $K_{12}=0.0012$ ps^{-1}. The intersubband scattering rate is much smaller than the intrasubband scattering rates. The corresponding subband mobilities are $\mu_1=270\,000$ cm^2/V s and $\mu_2=110\,000$ cm^2/V s. These values explain why in SdH measurements oscillations arising from the subband with population N_1 are observed at lower magnetic fields than those from the subband with population N_2. In the second configuration with $V_{TG}=1$ V, $N=2.3\times10^{11}$ cm^{-2} [Fig. 2(b1)], the scattering rates are $K_1=0.033$ ps^{-1}, $K_2=0.064$ ps^{-1}, and $K_{12}=0.0086$ ps^{-1}. Again, the intersubband scattering rate is about 1 order of magnitude smaller than the scattering rates of individual subbands. However, as the density is reduced, we observe that the scattering rates of the individual subbands increase by less than a factor of 2, while the intersubband scattering rate increases by a factor of 7. Such a behavior can be related to the fact that the energy separation Δ_{SO} between the two spin-split bands decreases with density and, therefore, it is easier for the carriers to scatter from one subband to the other. By reducing the density, the parabolic feature in the magnetoresistance around $B=0$ becomes broader and shallower.

We have also observed that an increase of the temperature causes a broadening of the magnetoresistance minimum around $B=0$ and also an increase of the intersubband scattering rate. The intersubband scattering rate increases faster with increasing temperature than the intrasubband scattering rates. This indicates that the presence of the two spin-split subbands in *p*-type samples might be relevant for the strong temperature dependence of the resistivity even at milliKelvin temperatures.[26–28]

Besides the longitudinal magnetoresistance minimum around $B=0$, the presence of the two spin-split subbands also modifies the Hall resistivity around $B=0$ and introduces nonlinear corrections [see Eq. (2)].[25] We have calculated the Hall resistivity using the scattering rates K_1, K_2, and K_{12} obtained from the ρ_{xx} fits as input parameters. In order to make these small nonlinear corrections to the Hall resistivity visible, we subtract the linear contributions from both the measured data and the calculated ρ_{xy}. The result for the measured data (black lines) and the calculated ρ_{xy} (gray lines) is presented in Fig. 2(a2) (configuration $V_{TG}=0$, $N=3.0\times10^{11}$ cm^{-2}) and Fig. 2(b2) (configuration $V_{TG}=1$ V, $N=2.3\times10^{11}$ cm^{-2}). We find reasonable agreement between the data and the simulated nonlinear corrections of the Hall resistivity.

V. WEAK ANTILOCALIZATION MEASUREMENTS

Weak (anti)localization effects are observable in lower mobility samples in the diffusive transport regime, if the carrier mean free path is much smaller than the phase-coherence length. In higher mobility samples where $k_F l_m \gg 1$ (k_F is the Fermi wave vector and l_m the mean free path), localization effects are weaker and harder to resolve. The measured density and mobility values in the investigated sample give $k_F l_m \sim 100-200$. Therefore, the magnitude of the localization effects is expected to be very small. In order to resolve a weak antilocalization peak in the magnetoresistivity, we had to determine both the resistance and the magnetic field in the narrow B-field range around $B=0$ with very high accuracy.

In the left column of Fig. 3, the raw magnetoresistivity data are presented for the gate configurations $V_{TG}=0$, $N=3\times10^{11}$ cm^{-2}, $\mu=160\,000$ cm^{-2}/V s, $k_F l_m=200$ [Fig. 3 (a1)] and $V_{TG}=1$ V, $N=2.3\times10^{11}$ cm^{-2}, $\mu=130\,000$ cm^{-2}/V s, $k_F l_m=120$ [Fig. 3 (b1)]. The presented data are obtained from symmetrizing the raw data for the sake of better stability of the fitting procedure presented below. In both cases, we observe a sharp antilocalization resistance minimum around B

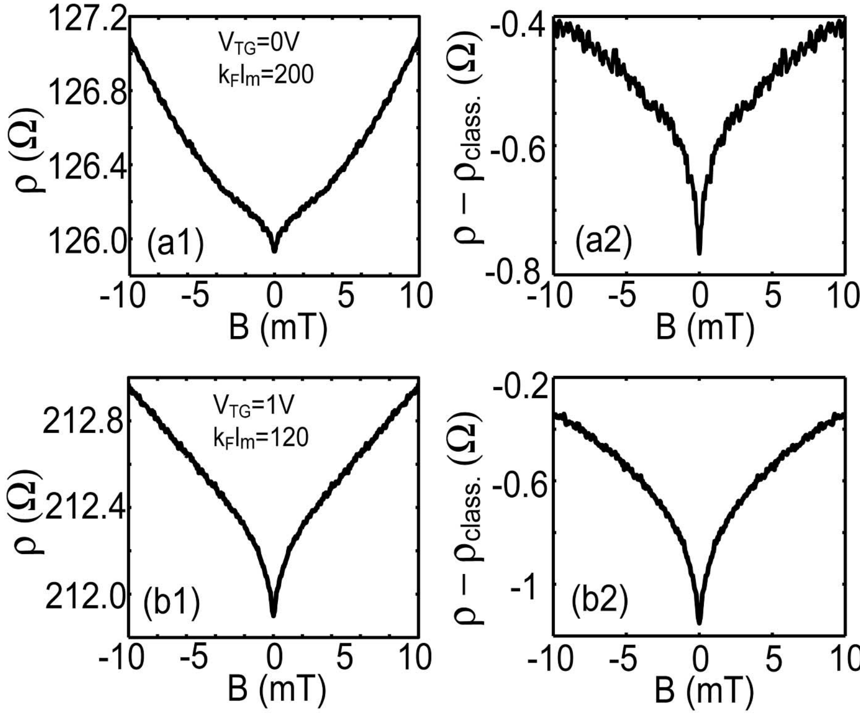

FIG. 3. Left column: Raw magnetoresistivity data (symmetrized) at $T=65$ mK in the following gate configurations: (a1) $V_{\mathrm{TG}}=0$, $N=3\times10^{11}$ cm^{-2}, $\mu=160\,000$ cm^{-2}/V s; (b1) $V_{\mathrm{TG}}=1$ V, $N=2.3\times10^{11}$ cm, $\mu=130\,000$ cm^{-2}/V s. Right column: Quantum correction of the resistivity obtained after subtraction of the classical two-band positive magnetoresistivity for (a2) $V_{\mathrm{TG}}=0$ and (b2) $V_{\mathrm{TG}}=1$ V.

$=0$ with a magnitude much smaller than 1 Ω. It can be seen that the magnitude and the width of the antilocalization minimum become larger as the factor $k_F l_m$ decreases due to a reduction of the sample mobility and density at positive top gate.

As discussed before, a classical magnetoresistance minimum is present around $B=0$ due to the presence of the two spin-split subbands. In order to separate the quantum correction from the low-field magnetoresistivity, we subtract the classical positive magnetoresistivity ρ_{class} [thick gray lines in Figs. 2(a1) and 2(b1)] from the total resistivity ρ. The quantum corrections to the resistivity, $\rho-\rho_{\mathrm{class}}$, are plotted in the right column of Fig. 3 for both gate configurations.

It can be seen in Figs. 3(a2) and 3(b2) that in both cases, a well developed weak antilocalization minimum is present in the low-field magnetoresistance. The fact that the narrow weak antilocalization minimum is not superimposed on a wider weak localization peak confirms that spin-orbit interactions in the system are exceptionally strong.[8,12]

In order to proceed with fitting the data with the Hikami–Larkin–Nagaoka (HLN) theory,[7] we need to calculate the conductivity correction

$$\Delta\sigma(B)=[\sigma(B)-\sigma(0)]-[\sigma_{\mathrm{class}}(B)-\sigma_{\mathrm{class}}(0)], \qquad (3)$$

where σ is the longitudinal conductivity, obtained from the inversion of the measured resistivity tensor, and σ_{class} is the classical longitudinal conductivity, obtained from the fitted ρ_{class}. The obtained conductivity correction $\Delta\sigma(B)$ is plotted in Fig. 4. The dots represent the measured data and the full lines are fits of the HLN theory for the top-gate configurations $V_{\mathrm{TG}}=1$ V, $k_F l_m=120$ (gray) and $V_{\mathrm{TG}}=0$, $k_F l_m=200$ (black). Strictly speaking, the HLN theory is valid in the diffusive regime, where $B<B_{\mathrm{tr}}=\hbar/(2el_m^2)$. In the case of the investigated sample, we have $B_{\mathrm{tr}}<0.3$ mT. The fitting interval shown in Fig. 4 is taken to be slightly larger than this value in order to include a reasonable number of points. The data are fitted with the expression for strong SOI in the limit $B\ll B_\phi$,[7,29]

$$\Delta\sigma(B)=-\frac{e^2}{\pi h}\left[\frac{1}{2}\Psi\left(\frac{1}{2}+\frac{B_\phi}{B}\right)-\frac{1}{2}\ln\frac{B_\phi}{B}\right], \qquad (4)$$

where $\Psi(x)$ is the digamma function, $B_\phi=\hbar/(4De\tau_\phi)$, D is the diffusion constant, and τ_ϕ is the phase-coherence time. The only fitting parameter is B_ϕ. Satisfactory fitting is obtained (full lines in Fig. 4) for both top-gate configurations, and the phase-coherence time of holes is extracted. In con-

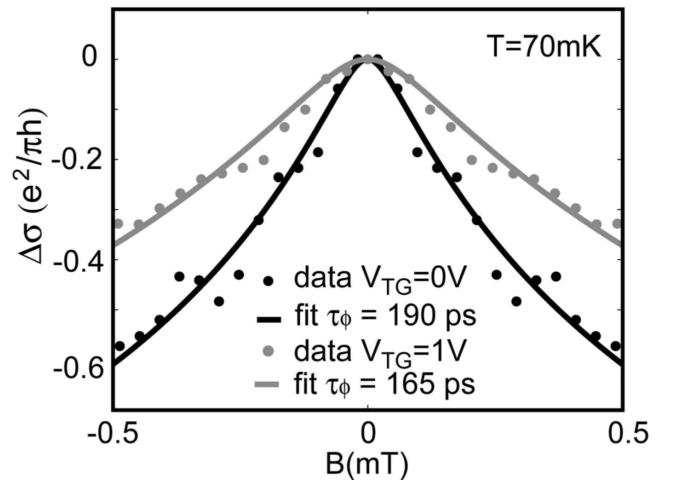

FIG. 4. Fit of the antilocalization conductance peak with the HLN theory [Eq. (4)]—full lines are fitted curves and points are experimental data for the top-gate configurations $V_{\mathrm{TG}}=1$ V, $k_F l_m=120$ (gray) and $V_{\mathrm{TG}}=0$, $k_F l_m=200$ (black).

figuration $V_{TG}=1$ V, $k_F l_m=120$ (gray points), we obtain $B_\phi = 5.1\times10^{-5}$ T, $\tau_\phi=165$ ps, and in configuration $V_{TG}=0$, $k_F l_m=200$ (black points), we obtain $B_\phi=2.6\times10^{-5}$ T, $\tau_\phi = 190$ ps. The corresponding phase-coherence lengths l_ϕ of holes, calculated according to the diffusive regime expression $l_\phi=\sqrt{D\tau_\phi}$, are 1.8 and 2.5 μm, respectively. These values show that the phase-coherence length of holes decreases as the density in the sample is reduced. The values are compatible with those obtained from measurements of Aharonov–Bohm oscillations in *p*-type GaAs rings.[30] They demonstrate that the fabrication of phase-coherent *p*-type GaAs nanostructures is accessible with present nanofabrication technologies. However, the values of l_ϕ in hole systems are approximately 1 order of magnitude smaller than in electron systems with comparable densities and mobilities.[31,32] Such a tendency was also observed in recent measurements of dephasing times of holes in open quantum dots.[33] It suggests stronger charge dephasing in hole than in electron systems, presumably due to stronger carrier-carrier interactions.[34]

Figure 5(a) shows the temperature evolution of the resistivity around $B=0$ in the top-gate configuration $V_{TG}=1$ V, $k_F l_m=120$. The antilocalization dip depends strongly on temperature and disappears completely above 300 mK, compatible with the temperature evolution of the Aharonov–Bohm oscillations in *p*-type GaAs rings.[30] In addition, the resistance at $B=0$ exhibits a metallic behavior with the zero-field resistivity increasing with temperature.

The fitting of the antilocalization peak in the conductance is performed for each measured temperature and the phase-coherence times are extracted. The inset of Fig. 5(b) shows fits obtained for temperatures of 70 and 190 mK, from which the phase-coherence times $\tau_\phi=165$ ps and $\tau_\phi=53$ ps, respectively, are extracted. It can be seen in Fig. 5(b) that the dephasing rate τ_ϕ^{-1} depends almost linearly on temperature.

Before we proceed with the evaluation of the spin-orbit scattering time τ_{SO} from weak antilocalization measurements, we estimate τ_{SO} from SdH measurements. The estimated spin-orbit-induced splitting of the heavy hole band at a density of $N=2.3\times10^{11}$ cm^{-2} is $\Delta_{SO}=0.47$ meV [Fig. 1(b)]. In semiconductor heterostructures with inversion asymmetry, the dominant spin-orbit relaxation mechanism is the Dyakonov–Perel mechanism,[35] which leads to the relation $\tau_{SO}^{-1}=\Delta_{SO}^2\tau_{tr}/4\hbar^2$.[35] Inserting the Drude transport scattering time $\tau_{tr}=26$ ps, we estimate $\tau_{SO}\sim0.3$ ps. This shows that the SOI is so strong that $\tau_{SO}\ll\tau_{tr}$. Therefore, the SOI cannot be treated as a weak perturbation, which is the common assumption in theoretical calculations. An estimate of the characteristic field $B_{SO}=\hbar/(4De\tau_{SO})$, at which the effects of SOI become suppressed and the weak antilocalization positive magnetoresistance turns into a weak localization negative magnetoresistance,[36] gives $B_{SO}\sim30$ mT, which is far beyond the transport field $B_{tr}\sim0.3$ mT up to which diffusive theories of weak antilocalization are applicable. However, the value $B_{SO}\sim30$ mT provides a qualitative understanding of the fact that we only observe a weak antilocalization dip without a weak localization peak in the measured magnetoresistivity.

We show the results of fitting the data in a wide magnetic field range with the HLN theory using the expression[7,36,37]

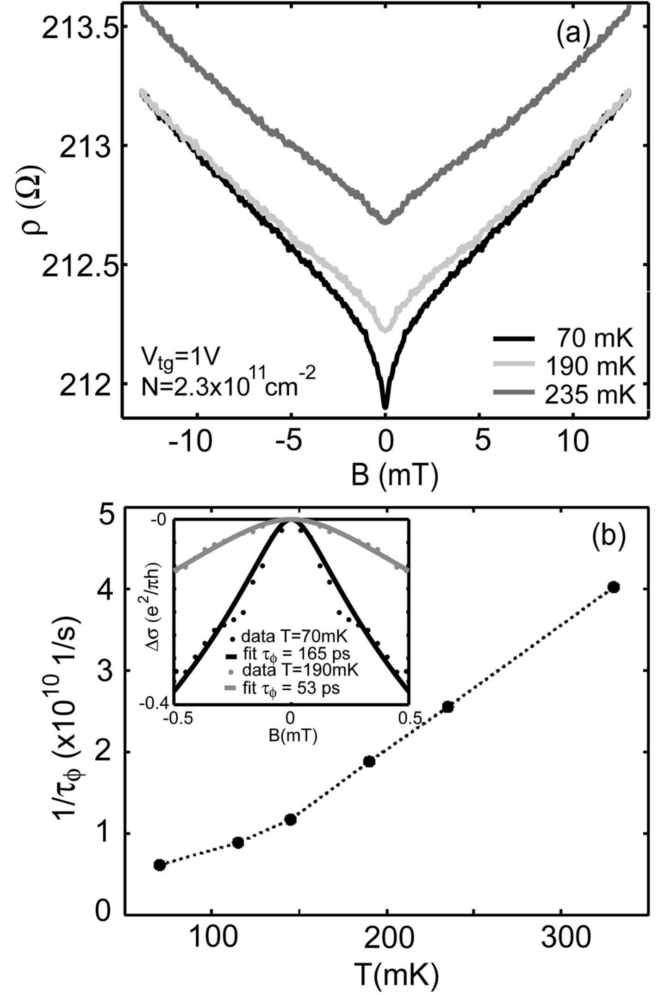

FIG. 5. (a) Temperature dependence of the antilocalization resistivity minimum in the top-gate configuration $V_{TG}=1$ V, $k_F l_m = 120$. (b) Temperature dependence of the inverse phase-coherence time of holes. Inset: Fit of the antilocalization conductance peak with the HLN theory [Eq. (4)] for temperatures of 70 mK (black) and 190 mK (gray)—full lines are fitted curves and points are experimental data.

$$\Delta\sigma(B) = -\frac{e^2}{\pi h}\left[\frac{1}{2}\Psi\left(\frac{1}{2}+\frac{B_\phi}{B}\right)-\frac{1}{2}\ln\frac{B_\phi}{B} - \Psi\left(\frac{1}{2}+\frac{B_\phi+B_{SO}}{B}\right)+\ln\frac{B_\phi+B_{SO}}{B} - \frac{1}{2}\Psi\left(\frac{1}{2}+\frac{B_\phi+2B_{SO}}{B}\right)+\frac{1}{2}\ln\frac{B_\phi+2B_{SO}}{B}\right]. \tag{5}$$

It should be mentioned that the HLN theory was originally developed for metallic samples where the Elliot spin-orbit (SO) skew-scattering mechanism is present. For this mechanism, the spin-splitting energy is proportional to k^3. However, in most semiconductor heterostructures, the Dyakonov–Perel spin relaxation is dominant.[35] The theory by Iordanskii–Lyanda-Geller–Pikus (ILP) describes the weak antilocalization correction for this type of spin relaxation,

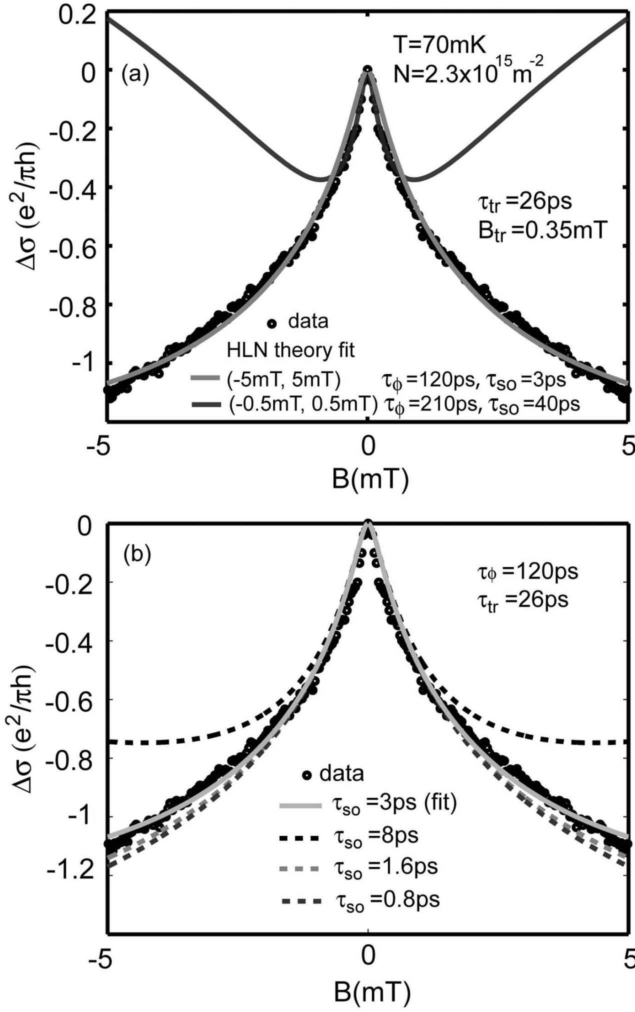

FIG. 6. (a) Fits of the weak antilocalization conductance peak with the HLN theory including SOI [Eq. (5)] in the range $|B| < 0.5$ mT (dark gray line) and in the range $|B| < 5$ mT (light gray line). (b) Sensitivity of the fits in the range $|B| < 5$ mT to the change of τ_{SO} [the full gray line represents the fit obtained in (a), while dashed lines correspond to different values of τ_{SO}, as quoted in the figure].

and it involves both linear and cubic in k spin-splitting terms.[37] If the linear contribution is negligible and the cubic spin-splitting is dominant, the ILP theory gives the same result as the HLN theory in Eq. (5).[36,37] Since the spin-orbit-induced splitting of the heavy hole GaAs band is proportional to k^3,[3,21] it is appropriate to use the HLN equation [Eq. (5)] for fitting the weak antilocalization in hole systems. Equation (5) contains two fitting parameters, namely, B_ϕ and B_{SO}.

The sharpness of the weak antilocalization conductance peak is determined by τ_ϕ, whereas the tail of the peak depends on τ_{SO}.[29,36] Therefore, we explore in Fig. 6(a) how the fit of the data with Eq. (5) depends on the magnetic field range. Fitting in the narrow range $|B| < 0.5$ mT [dark gray line in Fig. 6(a)] reproduces the low-field behavior quite well up to $B \sim B_{tr}$, but above that field, the fit does not match the experimental data. The obtained fitting parameters are in this case $\tau_\phi = 210$ ps and $\tau_{SO} = 40$ ps. On the other hand, the fit of the data in the larger range $|B| < 5$ mT [light gray line in Fig. 6(a)] matches the tails of the peak better but does not fit the low-field data below B_{tr} satisfactorily. The fit parameters in this second case are $\tau_\phi = 120$ ps and $\tau_{SO} = 3$ ps. While the obtained values for τ_ϕ differ by less than a factor of 2 and are comparable to the value obtained by fitting with Eq. (4) which does not contain τ_{SO}, the obtained values for τ_{SO} differ by more than an order of magnitude. Although the fit in the range $|B| < 0.5$ mT, i.e., below B_{tr}, is theoretically more justified, it is clear that it underestimates the SO strength because it gives an upturn from weak antilocalization to weak localization, which is not observed in the measured data. Also, the value $\tau_{SO} = 40$ ps is significantly larger than that estimated from the beating of the SdH oscillations $\tau_{SO} = 0.3$ ps. Fitting in the range $|B| < 5$ mT gives better agreement between the extracted $\tau_{SO} = 3$ ps and the value obtained from SdH oscillations. In Fig. 6(b), we investigate the influence of changing τ_{SO} at fixed $\tau_\phi = 120$ ps on the fitted curves and find that the fitting procedure becomes less sensitive for $\tau_{SO} < 3$ ps. Therefore, rather than giving the exact value, this fit sets the upper limit on τ_{SO}.

It should be mentioned that even admitting anisotropic spin relaxation and using the theory of Ref. 38 with three, instead of two, fitting parameters did not give better fits to the data. Also, curves simulated using the theory developed for the ballistic regime[39] could not satisfactorily match the data in the entire investigated magnetic field range.

Due to the exceptionally strong SOI effects and the high mobility of holes in our p-type GaAs sample, it is in the regime where $\tau_{SO} \ll \tau_{tr} \ll \tau_\phi$ ($\tau_{SO} \sim 0.3$ ps, $\tau_{tr} = 26$ ps, $\tau_\phi = 165$ ps). In this regime, SOI cannot be treated perturbatively, as it is the case in the more commonly studied regime $\tau_{tr} \ll \tau_{SO} \ll \tau_\phi$, where a small and sharp weak antilocalization resistance minimum is superimposed on a wider weak localization resistance peak. This might explain the difficulties in fitting our weak antilocalization data in a larger magnetic field range with present theoretical models. Similar difficulties in fitting weak antilocalization data were observed for an InGaAs/InP quantum well with strong SOI.[40]

It is also possible that the difficulties in fitting the weak antilocalization data arise from the fact that the low-field magnetoresistance contains some other contribution, in addition to the weak antilocalization, presumably due to carrier-carrier Coulomb interactions.[29] These interaction corrections might be particularly strong in p-type GaAs systems due to the effective mass of holes, which is significantly larger than in n-GaAs systems.

VI. CONCLUSIONS

In conclusion, we have performed a detailed analysis of the low-field magnetoresistance in a carbon-doped p-type GaAs heterostructure. The presence of exceptionally strong spin-orbit interactions in the structure is demonstrated by the simultaneous observation of a beating of SdH oscillations, a classical positive magnetoresistance, and a weak antilocalization correction in the magnetoresistance. A spin-orbit-induced heavy hole subband splitting of around 30% of the Fermi energy is deduced from the beating of SdH oscilla-

tions. The classical positive magnetoresistance, originating from the presence of the two spin-split subbands, has been fitted with a two-band model up to the fields where SdH oscillations are not yet developed, allowing to estimate the inter- and intrasubband scattering rates. In a very narrow magnetic field range around $B=0$, a weak antilocalization resistivity minimum is observed. The fact that this minimum is not superimposed on a wider weak localization peak confirms that the sample is in the regime where $\tau_{SO} \ll \tau_{tr} \ll \tau_{\phi}$, i.e., where spin-orbit interactions are very strong and cannot be treated perturbatively in calculations of quantum corrections of the magnetoresistance. From weak antilocalization measurements, the phase-coherence time of the holes is determined to be around 190 ps at $T=70$ mK. The temperature dependence reveals that the weak antilocalization resistance minimum persists up to 300 mK and that τ_{ϕ}^{-1} depends on temperature in an almost linear fashion. The extracted phase-coherence length of holes of around 2.5 μm at $T=70$ mK shows that the fabrication of phase-coherent *p*-type GaAs nanodevices is possible using present nanofabrication technologies.

ACKNOWLEDGMENTS

We thank L. Golub and M. Glazov for stimulating discussions. Financial support from the Swiss National Science Foundation is gratefully acknowledged.

[1] G. Dresselhaus, Phys. Rev. **100**, 580 (1955).
[2] Y. A. Bychkov and E. I. Rashba, J. Phys. C **17**, 6039 (1984); JETP Lett. **39**, 78 (1984).
[3] R. Winkler, *Spin-Orbit Coupling Effects in Two-Dimensional Electron and Hole Systems*, Springer Tracts in Modern Physics Vol. 191 (Springer-Verlag, Berlin, 2003).
[4] W. Zawadzki and P. Pfeffer, Semicond. Sci. Technol. **19**, R1 (2004).
[5] C. W. J. Beenakker and H. van Houten, Solid State Phys. **44**, 1 (1991).
[6] G. Bergmann, Solid State Commun. **42**, 815 (1982).
[7] S. Hikami, A. I. Larkin, and Y. Nagaoka, Prog. Theor. Phys. **63**, 707 (1980).
[8] G. Bergmann, Phys. Rev. Lett. **48**, 1046 (1982).
[9] D. A. Poole, M. Pepper, and A. Hughes, J. Phys. C **15**, L1137 (1982).
[10] P. D. Dresselhaus, C. M. A. Papavassiliou, R. G. Wheeler, and R. N. Sacks, Phys. Rev. Lett. **68**, 106 (1992).
[11] G. L. Chen, J. Han, T. T. Huang, S. Datta, and D. B. Janes, Phys. Rev. B **47**, 4084 (1993).
[12] T. Koga, J. Nitta, T. Akazaki, and H. Takayanagi, Phys. Rev. Lett. **89**, 046801 (2002).
[13] S. Pedersen, C. B. Sörensen, A. Kristensen, P. E. Lindelof, L. E. Golub, and N. S. Averkiev, Phys. Rev. B **60**, 4880 (1999).
[14] Y. Yaish, O. Prus, E. Buchstab, G. Ben Yoseph, U. Sivan, I. Ussishkin, and A. Stern, arXiv:cond-mat/0109460 (unpublished).
[15] S. J. Papadakis, E. P. De Poortere, H. C. Manoharan, J. B. Yau, M. Shayegan, and S. A. Lyon, Phys. Rev. B **65**, 245312 (2002).
[16] A. D. Wieck and D. Reuter, *Proc Int. Conf. on Compound Semiconductors 1999*, Berlin, Germany, Inst. Phys. Conf. Ser. 166 (Institute of Physics, Bristol and Philadelphia, 1976), p. 51.
[17] B. Grbić, C. Ellenberger, T. Ihn, K. Ensslin, D. Reuter, and A. D. Wieck, Appl. Phys. Lett. **85**, 2277 (2004).
[18] B. Grbić, Ph.D. thesis, ETH Zurich, 2007.
[19] J. J. Heremans, M. B. Santos, K. Hirakawa, and M. Shayegan, J. Appl. Phys. **76**, 1980 (1994).
[20] J. P. Lu, J. B. Yau, S. P. Shukla, M. Shayegan, L. Wissinger, U. Rössler, and R. Winkler, Phys. Rev. Lett. **81**, 1282 (1998).
[21] L. G. Gerchikov and A. V. Subashiev, Sov. Phys. Semicond. **26**, 73 (1992).
[22] J. P. Eisenstein, H. L. Störmer, V. Narayanamurti, A. C. Gossard, and W. Wiegmann, Phys. Rev. Lett. **53**, 2579 (1984).
[23] B. Habib, E. Tutuc, S. Melinte, M. Shayegan, D. Wasserman, S. A. Lyon, and R. Winkler, Phys. Rev. B **69**, 113311 (2004).
[24] N. W. Ashcroft and N. D. Mermin, *Solid State Physics* (HRW International Editions, Philadelphia, 1976).
[25] E. Zaremba, Phys. Rev. B **45**, 14143 (1992).
[26] S. S. Murzin, S. I. Dorozhkin, G. Landwehr, and A. C. Gossard, JETP Lett. **67**, 113 (1998).
[27] S. J. Papadakis, E. P. De Poortere, H. C. Manoharan, M. Shayegan, and R. Winkler, Science **283**, 2056 (1999).
[28] Y. Yaish, O. Prus, E. Buchstab, S. Shapira, G. Ben Yoseph, U. Sivan, and A. Stern, Phys. Rev. Lett. **84**, 4954 (2000).
[29] B. L. Altshuler, A. G. Aronov, A. I. Larkin, and D. E. Khmelnitskii, Sov. Phys. JETP **54**, 411 (1981).
[30] B. Grbić, R. Leturcq, T. Ihn, K. Ensslin, D. Reuter, and A. D. Wieck, Phys. Rev. Lett. **99**, 176803 (2007).
[31] T. Ihn, A. Fuhrer, M. Sigrist, K. Ensslin, W. Wegscheider, and M. Bichler, Adv. Solid State Phys. **43**, 139 (2003).
[32] A. E. Hansen, A. Kristensen, S. Pedersen, C. B. Sørensen, and P. E. Lindelof, Phys. Rev. B **64**, 045327 (2001).
[33] S. Faniel, B. Hackens, A. Vlad, L. Moldovan, C. Gustin, B. Habib, S. Melinte, M. Shayegan, and V. Bayot, Phys. Rev. B **75**, 193310 (2007).
[34] G. Seelig and M. Büttiker, Phys. Rev. B **64**, 245313 (2001).
[35] M. I. Dyakonov and V. I. Perel', Sov. Phys. JETP **33**, 1053 (1971).
[36] W. Knap, C. Skierbiszewski, A. Zduniak, E. Litwin-Staszewska, D. Bertho, F. Kobbi, J. L. Robert, G. E. Pikus, F. G. Pikus, S. V. Iordanskii, V. Mosser, K. Zekentes, and Yu. B. Lyanda-Geller, Phys. Rev. B **53**, 3912 (1996).
[37] S. V. Iordanskii, Yu. B. Lyanda-Geller, and G. E. Pikus, JETP Lett. **60**, 204 (1994).
[38] N. S. Averkiev, L. E. Golub, and G. E. Pikus, JETP **86**, 780 (1998).
[39] L. E. Golub, Phys. Rev. B **71**, 235310 (2005); M. M. Glazov and L. E. Golub, Semiconductors **40**, 1209 (2006).
[40] S. A. Studenikin, P. T. Coleridge, G. Yu, and P. J. Pole, Semicond. Sci. Technol. **20**, 1103 (2005).